Full length article

Disorder to order transition in cell-ECM systems mediated by cell-cell collective interactions

Umnia Doha, Onur Aydin, Md Saddam Hossain Joy, Bashar Emon, William Drennan, M. Taher A. Saif*

Department of Mechanical Science and Engineering, University of Illinois Urbana Champaign, United States

ABSTRACT

Cells in functional tissues execute various collective activities to achieve diverse ordered processes including wound healing, organogenesis, and tumor formation. How a group of individually operating cells initiate such complex collective processes is still not clear. Here, we report that cells in 3D extracellular matrix (ECM) initiate collective behavior by forming cell-ECM network when the cells are within a critical distance from each other. We employed compaction of free-floating (FF) 3D collagen gels with embedded fibroblasts as a model system to study collective behavior and found a sharp transition in the amount of compaction as a function of cell-cell distance, reminiscent of phase transition in materials. Within the critical distance, cells remodel the ECM irreversibly, and form dense collagen bridges between each other resulting in the formation of a network. Beyond the critical distance, cells exhibit Brownian dynamics and only deform the matrix reversibly in a transient manner with no memory of history, thus maintaining the disorder. Network formation seems to be a necessary and sufficient condition to trigger collective behavior and a disorder-to order transition.

Statement of significance

Macroscopic compaction of *in vitro* collagen gels is mediated by collective mechanical interaction of cells. Previous studies on cell-induced ECM compaction suggest the existence of a critical cell density and phase transition associated with this phenomenon. Cell-mediated mechanical remodeling and global compaction of ECM has mostly been studied at steady state. Our study reveals a link between a transition in cell dynamics and material microstructure as cells collectively compact collagen gels. It underscores the significance of temporal evolution of these cell-ECM systems in understanding the mechanism of such collective action and provides insights on the process from a mechanistic viewpoint. These insights can be valuable in understanding dynamic pathological processes such as, cancer progression and wound healing, as well as engineering biomaterials and regenerative tissue mimics.

1. Introduction

Emergent behavior of multi-component systems results from coordination and interaction among constituting entities, which has distinct characteristics compared to individual component behavior. Such behavior is found in nature in a diverse range of organisms, such as- flocks of birds [1], schools of fishes [2], herds of sheep or colonies of ants. Collective motion and pattern formation is also observed in sub-tissue level cell organization during embryonic development and morphogenesis [3–6]. The under-

lying mechanism of the onset of collective behavior in multicellular systems is instrumental to understand physiological and pathological processes, such as-wound healing [7–9], tumor progression and metastasis during cancer development [10–12]. Several studies in the past have reported extrinsic or intrinsic critical parameters associated with transition from stochastic behavior of individual cells to population-level ordered collective activity in a variety of multicellular systems including collective migration of epithelial cells [13,14], synchronous firing of neurons [15], vasculature formation by endothelial cells [16] and population-level rhythmic activity of social amoeba [17]. All of these studies have identified cell density as a general critical parameter associated with this behavioral transition. This transition from disordered to ordered state in cellular activity as a collective behavior emerges is reminiscent of material

phase transitions in physical systems. A structural method to establish physical parameters that describe phase transition in multicellular living systems has been developed by Yang et al. in a recent study [18]. Grekas et al. [19] proposed a bistable energy-based model for phase transition in fibrous ECM remodeled by cells that is analogous to austenite-martensite transformation in metals [20]. However, a mechanistic origin of this cellular phase transition and how it is associated with a critical cell density is not well understood.

Biopolymer network-based 3D *in vitro* platforms such as- collagen, fibrin or reconstituted basement membrane matrix have emerged as an excellent tissue mimics to study cell response to various mechanical signaling arising from cell-ECM interactions. With such a platform first developed by Bell et al. [21] by embedding fibroblasts in a free-standing collagen lattice, subsequent studies have demonstrated that cells macroscopically compact the ECM by exerting contractile force [22,23]. This is attributed to permanent remodeling of collagen microenvironment by cells through interaction with the fibrous ECM. Contractile cells mechanically interact with the surrounding fibers by pulling onto them. The rich nonlinear mechanics of fibrous collagen networks enable long range cell-cell interaction through strain-stiffening of collagen [24–27]. To get insight into the mechanism of compaction of tissues, a number of models have been developed correlating global compaction to various phenomenon arising from local mechanical crosstalk between individual cells and ECM. Fiber alignment and contractile stress exerted by cells in response to mechanical stimuli [28], pericellular collagen concentration [29], and contact guidance [30,31] have been highlighted in previous studies. The seminal work by Bausch et al. [32] suggested that compaction results from collective mechanical activity of cells, where the authors measured contraction of a bounded collagen gel perpendicular and parallel to the boundary and deduced the role of nonlinear elasticity of collagen, cell orientation and cell density in regulating contraction. Their findings suggested a critical cell-cell distance of 100 μm for global contraction of collagen gel in their system. However, whether there is a threshold mechanical factor (e.g. cell force or ECM stiffness) corresponding to this critical cell-cell distance for global ECM remodeling remains unclear. Quantification of traction force of single and multiple cells embedded in 3D collagen lattice has revealed that force does not scale linearly with number of cells [33,34]. This implies that it is difficult to directly pinpoint one or more physical cues related to the critical cell density for ECM compaction, and spatiotemporal evolution of coordination in cellular interaction needs to be studied thoroughly to have a better understanding of the origin of this emergent behavior.

Here, we have developed a simple high throughput 3D platform for making free floating (FF) collagen gels to study the role of critical cell density in macroscopic compaction from a mechanical viewpoint. Our experimental platform enables us to gain insight on the temporal evolution of global compaction through the dynamic interplay between cell and ECM. Our experiments revealed the existence of a critical cell density needed for global compaction of free floating collagen gels. We have found striking structural differences in the microstructure of collagen gels with supercritical and subcritical cell densities. Using tracer beads, we showed that single cells exhibit a transient remodeling of ECM when cell density is below a critical value, whereas permanent remodeling of ECM through collective mechanical interaction is observed at cell density above the critical regime. By tracking the position of cells over time, we found a transition from Brownian to ballistic motion as cells compact the gel - a further evidence of a phase transition associated with global compaction. Finally we showed that this phase transition is mediated by mechanical interaction between cells by incorporating inert polystyrene (PS) beads along with cells in our system.

2. Materials and method

2.1. High throughput PDMS platform for free-floating collagen gel

We designed a 3D-printed mold for making FF collagen gels and an array of wells for imaging large number of samples simultaneously (Fig. 1A). Liquid polydimethylsiloxane (PDMS) (SYLGARD® 184- Sigma Aldrich, Saint Louis, MO) was poured in these 3D printed molds and cured at 60 °C overnight. The PDMS scaffolds for the FF gels and the imaging wells are then peeled off from the molds. Each scaffold contains 19 through-holes of 2 mm diameter and has a thickness of 500 μm (Fig. 1D). The imaging wells are 3 mm in diameter and 10 mm high and are connected by microfluidic channels at the bottom (Fig. 1B). The PDMS scaffolds and imaging wells were sterilized by autoclaving at 121 °C for 45 minutes. The imaging wells were attached to glass-bottom petri dishes and treated with O_2 plasma to render the PDMS surfaces hydrophilic and prevent the formation of air pockets after inundating with culture media. All PDMS structures were treated overnight with 2% w/v Pluronic® F-127 (Sigma Aldrich, St Louis, MO) to reduce collagen adhesion to PDMS and thereby facilitate the detachment of collagen gels from the scaffolds. The selected dimensions of the imaging wells ensure that the free-floating collagen gels are always confined to the field of view of our microscope objective during imaging. We can produce 19 gels from one scaffold and do time-lapse imaging of 19 wells containing gels with different cell densities simultaneously using a motorized stage (PRIOR Scientific, Rockland, MA). This experimental platform is simple to fabricate, yet highly efficient in terms of duration of experiments and sample yield. The main advantage of our 3D-printed platform over standard 96 or 384-wells plates is that it ensures that the floating discs are always confined within the field of view of a 4x objective while doing time lapse imaging. Also, it enables us to do time lapse imaging of a large number of samples using a standard motorized stage without the need for any additional fixtures to fit a standard 96 or 384-well plate in our microscope system.

2.2. Cell culture

We used NIH 3T3 fibroblasts(passage number 5-10) for our experiments. Cells were cultured in flasks in media consisting of 89% v/v Dulbecco's Modified Eagle's Medium (DMEM) (Corning® Inc., Corning, NY), 10% v/v Fetal Bovine Serum (FBS) (ThermoFisher Scientific™, Waltham, MA) and 1X Penicillin Streptomycin (Lonza®, Basel, Switzerland) until reaching 70-80% confluency. Cells were detached from the flasks using 0.05% Trypsin-EDTA (Gibco™, Waltham, MA) and centrifuged at 150 g for 5 minutes to obtain a cell pallet. The cells were next resuspended in cell culture media and counted using a hemocytometer (Hausser Scientific™). Next, cell suspension of double the desired cell densities were prepared with cell culture media.

2.3. Collagen preparation

Type I collagen with a density of 4mg/ml (Corning® Inc., Corning, NY) was prepared from a stock solution according to the manufacturer's protocol. Briefly, collagen was diluted with ice-cold deionized water and 10X phosphate buffer saline (PBS) (Lonza®, Basel, Switzerland). The solution was neutralized by adding 10N NaOH (Sigma Aldrich, Saint Louis, MO) to achieve a pH of 7.2-7.4.

2.4. FF collagen gel preparation

Equal volumes of collagen solution and cell suspension containing double the desired cell densities were mixed on ice to achieve a cell-collagen mixture of the desired density, with a final colla-
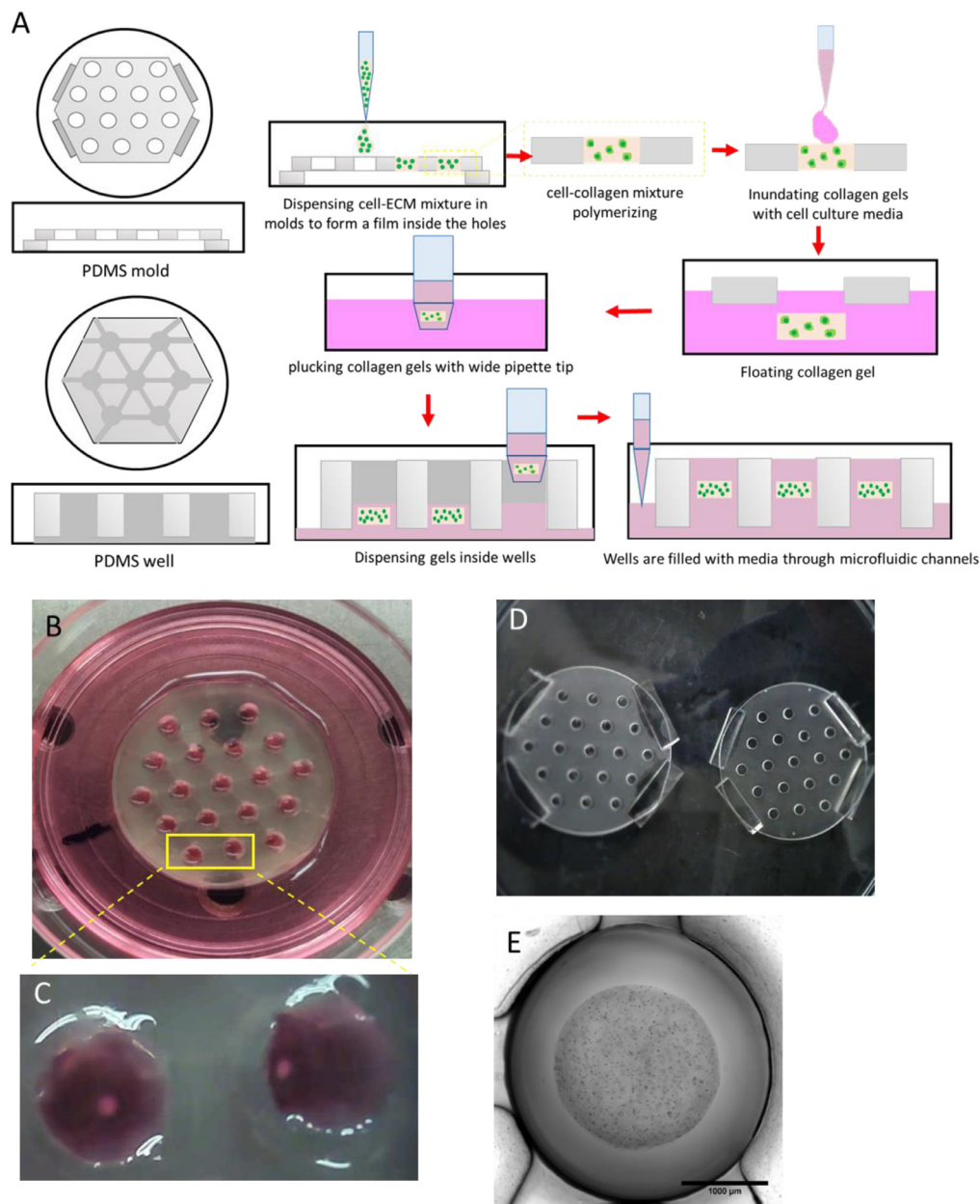
Fig. 1. High throughput platform for constructing and imaging collagen samples. **A.** Schematic diagram of the process flow for making 3D free-floating (FF) collagen discs. **B.** An array of PDMS wells. The wells are connected by microfluidic channel at the bottom to facilitate dispensing media inside the wells. **C.** Zoomed-in image of two wells containing collagen discs. **D.** PDMS scaffolds for making collagen discs. **E.** Bright field image of a free-floating collagen disc seeded with 3T3 fibroblast cells. Scale bar represents 1mm.

gen concentration of 2 mg/ml. The cell-collagen mixture was dispensed inside the holes of the PDMS scaffolds. The samples were then incubated at 37 °C for 25 minutes until the collagen solution polymerized, forming disc shaped gels. After polymerization, cell-culture media was poured on top of the discs to detach them from the Pluronic coated scaffolds. The scaffolds were removed, and free floating collagen discs were obtained. The discs were then taken out from the media using a wide-tip pipette and dispensed inside the imaging wells. The wells were then filled with a mixture of cell culture media and Percoll (Sigma Aldrich, Saint Louis, MO) to prevent the discs from sinking and settling at the bottom of the wells. Percoll results in a density gradient and lifts the FF discs above the floor.

2.5. PS bead preparation

Inert polystyrene (PS) beads (Bangs Laboratories, Fishers, IN) of 15 μm diameter were coated with collagen before mixing them with cell-collagen mixture according to manufacturer's protocol. Briefly, the desired volume of bead stock solution was centrifuged at 200g for 5 minutes to obtain a bead pallet with desired number of beads. After aspirating the liquid suspension, the bead pallet was re-suspended in 0.1% collagen solution in PBS for 20 minutes. This solution was then centrifuged again and the solvent was aspirated to obtain collagen-coated PS beads. For the experiments with different cell densities, a bead density of 1 million/ml of collagen was used.

2.6. Data acquisition and image analysis

Time-lapse imaging of FF discs with different cell densities were done using a 4x objective lens in an IX81 Olympus Microscope for 72 hours. The images were analyzed with ImageJ to measure the diameter of the collagen discs at different time points. Two photon Second Harmonic Generation (SHG) and confocal images of the FF discs were obtained using a LSM 710 microscope (Zeiss). Cell tracking was done using the open-source tracking software Tracker-Video Analysis and Modeling Tool. Temporal mean square displacement (tMSD) analysis was done using a custom MATLAB script. For the MSD analysis, cell tracking was done using ImageJ plugin Trackmate and MATLAB pre-class MSD analyzer [35].

2.7. Immunofluorescence assay

FF gels with super and subcritical cell densities were fixed and stained using a standard staining protocol. Briefly, samples were fixed with 4% v/v Paraformaldehyde (Electron Microscopy Sciences, Hatfield, PA) in PBS (ThermoFisher Scientific™, Waltham, MA). Next the samples were permeabilized in 0.1% v/v Triton™ X-100 (Sigma Aldrich, Saint Louis, MO) in PBS for 30 minutes. Blocking was done by incubating the samples in a solution containing 0.1% v/v Triton-X 100, 0.2% w/v bovine serum albumin (BSA) and 2% v/v natural goat serum in PBS for 1 hour. After rinsing the samples with PBS, conjugated antibody Phalloidin Alexa Fluor 647 (ThermoFisher Scientific™, Waltham, MA) was added to stain the cells for actin and kept in room temperature for 2 hours. Following rinsing with PBS, the nuclei were stained with DAPI (Sigma Aldrich, Saint Louis, MO) for 10 minutes. A final rinsing was done with PBS to complete the staining procedure. All the steps were performed at room temperature.

For the cell-bead experiments, live cell imaging was done by using green cell tracker (ThermoFisher Scientific™, Waltham, MA). After detaching the cells from the culture flask, they were incubated in 5 mM green cell-tracker solution (serum free media) for 45 minutes at 37 °C. After that, the media was removed, and cells were suspended in cell culture media and collagen to form the FF discs as described above. Live imaging for cell tracking experiments was done by labeling the nuclei with a far red flourescent SiR DNA kit (Cytoskeleton Inc., Denver, CO). The cells were incubated in phenol red-free culture media containing the staining reagent prepared according to the manufacturer's protocol.

2.8. Quantification of fiber orientation

Fiber orientation was quantified by nematic order parameter (NOP) using the ImageJ plugin OrientationJ [36]. For perfectly isotropic and anisotropic material, the value of NOP is 0 and 1, respectively. Angular distribution of collagen intensity in circular region of interest (ROI) was determined using custom MATLAB scripts.

2.9. Scanning Electron Microscopy (SEM) of collagen gels

SEM imaging of the collagen discs was done following the protocol described in [37]. Briefly, collagen disks of different cell densities were fixed with 4% PFA (paraformaldehyde) for 1 hour at room temperature. The samples were then washed three times, 10 minutes each, in PBS and two times, 10 minutes each, in bio-grade water (Corning Inc., NY). After that, samples were transferred to a glass vial containing 1% Osmium Tetroxide (Electron Microscopy Sciences, Hatfield, PA) and incubated for 1 hour at room temperature. Following Osmium Tetroxide fixation, dehydration of the samples was done in graded water/ethanol series (10 minutes of washing in 30%, 50%, 70%, 90%, and two 100% ethanol). Then the

samples were washed with graded ethanol/HMDS (Electron Microscopy Sciences, Hatfield, PA) solution (15 minutes of washing in 33%, 50%, 66%, and 100% HMDS). Finally, the samples were allowed to dry overnight at room temperature. The dried sample was then coated with Pd/Au using the Denton Desk II TSC turbo-pumped sputter coater (Denton Vacuum, Inc., USA). The SEM imaging was done using FEI Quanta FEG 450 ESEM (FEI Company, USA).

2.10. Statistics

All data presented here except for the single cell and bead tracking are in terms of mean ± SD. Student t-test was done for the quantification of NOP where $p < 0.01$ is considered as statistically significant.

3. Results

3.1. A critical cell-cell distance exists for cell-mediated compaction of FF collagen discs

In order to test whether there is a critical cell density above which cells compact the FF discs, we seeded them with 3T3 fibroblast cells of various initial densities, and measured corresponding compaction of the discs by the cells. We formed collagen gels with 10 different cell densities (0.01-5 million/ml cells). Using our PDMS wells, we did time lapse imaging of multiple samples (n=6) for each cell density simultaneously for 72 hours and recorded the corresponding reduction in disc area due to compaction. Area of the discs at any time point are normalized by the initial area, which is same for all samples. Consistent with previous studies, we observed different shrinking rate for different cell densities during the first 72 hours (Fig. 2A, Supplementary Movie S.1-S.2). However when we measured the area reduction ratio (A/A_0) on day 11, we found a sharp distinction in distribution of samples with different initial cell densities. Samples with cell densities above 0.1 million cells/ml clustered around an area reduction ratio of 0.2, while samples with cell densities of 0.1 million/ml and below exhibited an approximate area reduction ratio of 1, i.e., their areas did not reduce (Fig. 2B). We estimated cell-cell distance from cell density by assuming cell-populated FF discs as uniform cubic lattice structures with cells at the vertices. The compaction parameter ($\psi = 1 - A/A_0$) vs cell-cell distance graphs at different time points reveal high degree of compaction ($\psi \approx 0.8$) when cell-cell distance is below a lower bound (160 μm), and negligible compaction ($\psi \approx 0$) when the distance exceeds an upper bound (210 μm, Fig. 2C). These bounds define a relatively small cell-cell distance regime (160-200 μm), indicating the existence of a critical cell-cell distance that separates two distinct cell-induced phenomena.

In order to assess the effect of cell proliferation and apoptosis on the initial cell density and concomitant compaction of the discs, we quantified both cell proliferation and cell death rate. Cell proliferation rate was quantified by counting the number of cells in collagen discs from bright field images taken every 24 hours after forming the discs. We repeated this for n=10 samples for up to 72 hours and found that cell density (million/ml) increases by approximately 5.5% on average in every 24 hours (Supplementary Information S.1, Fig. S.1). This suggests that rate of proliferation of 3T3 fibroblasts in 3D collagen is rather slow and the population doubling time for these cells is much longer compared to the duration of our experiment (72 hours). Cell viability was quantified by staining the nuclei of the dead cells in collagen discs at different time points using a cell viability assay kit (Abcam, MA). We found that the percentage of cell death during first 24-48 hours is approximately 8-9% (Supplementary Information S.2, Fig. S.2). Combining these two findings, we can infer that the rate of cell proliferation and apoptosis during the length of our experiment nul-
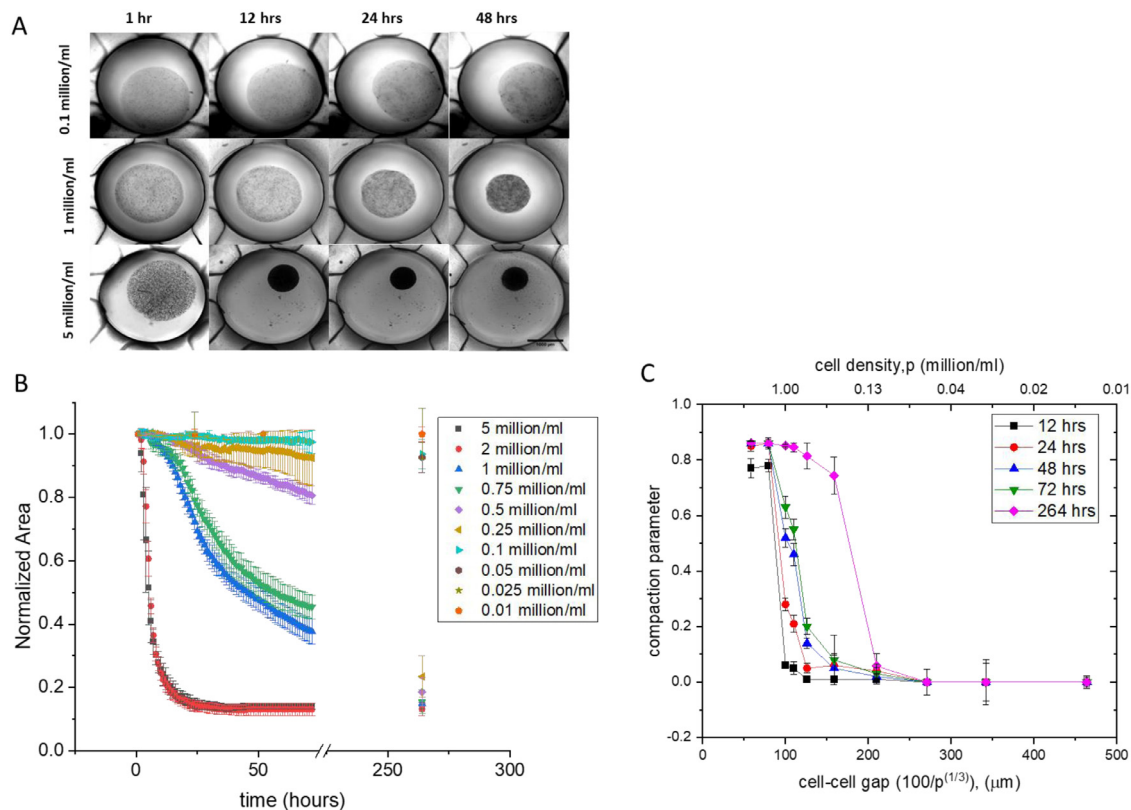
Fig. 2. Compaction of FF collagen discs seeded with different initial densities of 3T3 fibroblast cells. **A.** Bright field images of compaction process at different time points for 0.1, 1 and 5 million/ml cells. Collagen concentration is 2 mg/ml. Scale bar represents 1mm. **B.** Normalized area of FF collagen discs recorded continuously for 72 hours for different initial cell densities along with the data taken after 264 hours (11 days), each data point represents mean ± standard deviation of multiple (n=6) samples. **C.** Compaction parameter ψ as a function of cell-cell gap at different time points. A sudden drop in compaction is observed beyond a critical cell-cell distance at different time points.

lify each other and thus have a negligible effect on the total cell number. We also measured the change in thickness of the discs as a function of time and calculated the volumetric change from the reduction in thickness and area of the discs. We then estimated how cell-cell distance changes over time, assuming the number of cells in a disc remains constant over the duration of our experiment (72 hours). The results are presented in supplementary section (Supplementary Information S.6). Our findings on the existence of a critical cell density for compaction are consistent with previous studies that reported the cell-cell distance-dependence of different collective cellular processes [15,16,32]. However, the origin of this criticality for compaction remains elusive. We explored the mechanism next.

3.2. Formation of network of cells is associated with phase transition in collagen architecture

We next focused on examining the collagen microarchitecture of FF collagen discs with sub and supercritical cell densities. Samples of each category were fixed and stained for actin and nuclei at different time points. Confocal image of a disc with supercritical cell density (1 million/ml) fixed after 24 hours shows cells extend long actin-rich filopodial protrusions towards each other, forming a network-like structure. Second harmonic generation (SHG) image of collagen fibers in the same location reveals formation of collagen bands consisting of aligned fibers bridging the cells. Thus, a network like pattern consisting of densified collagen tracts as links with cells at the nodes emerges (Fig. 3A-C). Fiber alignment and formation of thick collagen bundles is mediated by cell-induced contractile force as reported in previous studies [19,38–40]. In con-

trast, cells in a subcritical sample (0.025 million/ml) after 72 hours had filopodial protrusions in random direction. The corresponding ECM microenvironment consists of a homogenous distribution of randomly oriented collagen fibers (Fig. 3E-G). Collagen densification has been quantified as a function of collagen intensity in SHG images previously [40]. To quantify the isotropy vs anisotropy in collagen microarchitecture, we measured collagen intensity from the SHG images in a circular region of interest (ROI) centering at the nuclei for both cases. We found that for supercritical cell density, collagen intensity values along the direction of filopodial protrusions are much higher than the mean intensity value of the ROI (Fig. 3D). For samples with subcritical cell-density, no significant peaks in collagen intensity distribution in the ROI was observed (Fig. 3H). We used nematic order parameter (NOP), which is a quantitative measure of fiber anisotropy- to assess the isotropic-anisotropic transition. The range of NOP varies from 0 to 1, signifying pure isotropy and anisotropy respectively. From the quantification of fiber orientation at different locations of the discs with both super and subcritical cell densities, we found that NOP is 0.45 and 0.12 for supercritical and subcritical cell density, respectively, suggesting the existence of isotropic to anisotropic transition in collagen microstructure (Fig. 3I). Formation and non-formation of cell-collagen network corresponding to super and subcritical cell density was also observed globally in gels from SHG images (Supplementary Information S.8, Fig. S.9), supporting our claim of global cell-ECM network formation consisting of fiber bridges when the collagen discs compact. We have also done SEM imaging of the discs of both categories to compare the dimensions of the collagen bridges with single collagen fibers (Fig. 3J-K, Supplementary Information S.9). Gerkas et al. showed formation of such collagen
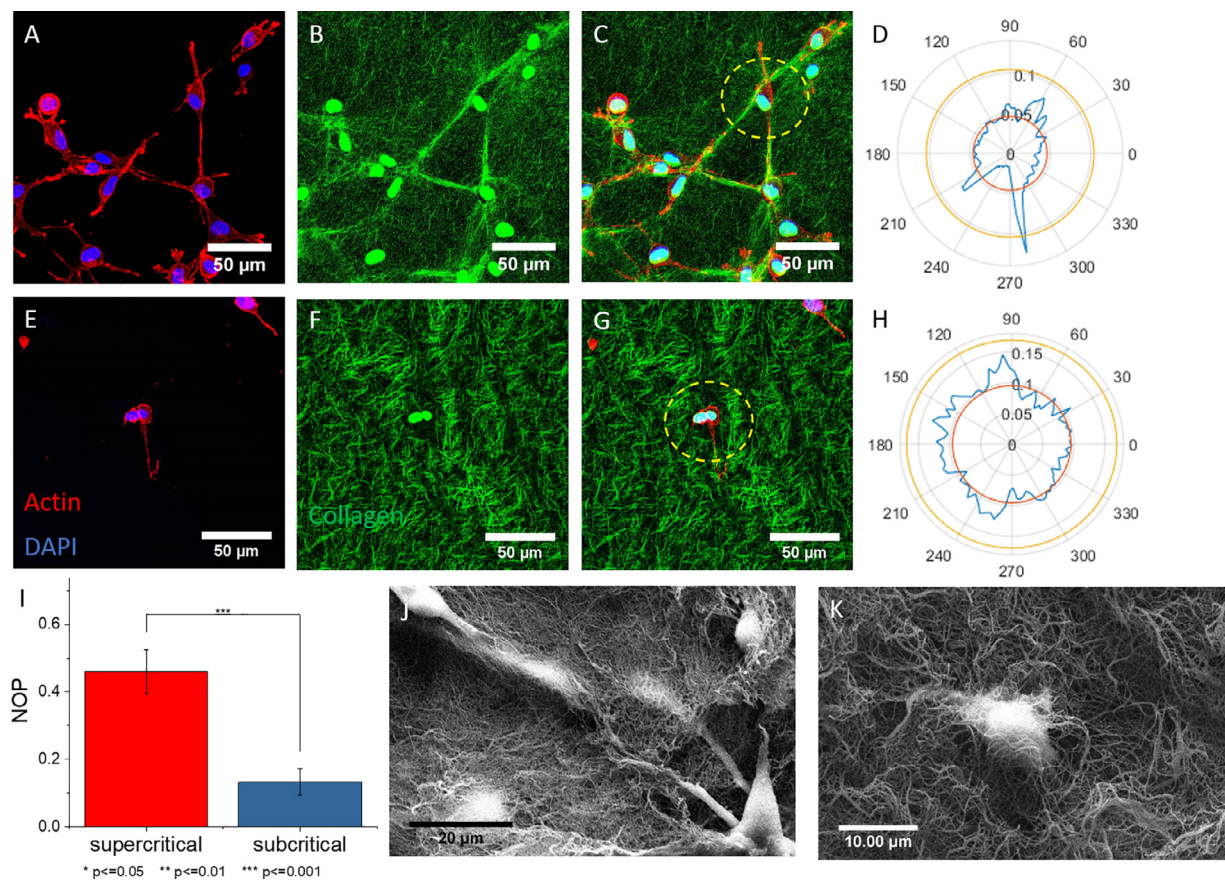
Fig. 3. Transition from disordered to ordered orientation of collagen fibers in FF discs with subcritical and supercritical cell density. **A.** Confocal image of multiple interacting cells extending filopodia towards each other in a supercritical sample (1 million/ml cells), fixed after 24 hours. **B.** Corresponding SHG image shows densified collagen bands aligned with the direction of cell protrusions. **C.** Superimposed image of cell and collagen fibers. **D.** Polar plot of the collagen intensity distribution in the ROI (marked by the yellow dotted circle in C), along with the mean intensity (red circle) and mean+SD (yellow circle) of the image. **E.** Confocal image of a single cell fixed after 72 hours in a subcritical sample (0.1 million/ml) protruding filopodia in random direction. **F.** Corresponding SHG image of homogeneous collagen fiber distribution. **G.** Superimposed image of cell in 3D collagen. **H.** Polar plot of the collagen intensity distribution in the ROI (marked by the yellow dotted circle in G), along with mean intensity (red circle) and mean+SD (yellow circle) of the entire iamge. **I.** Mean Nematic Order Parameter (NOP) of supercritical and subcritical cell density discs (n=20). Supercritical and subcritical samples has a mean NOP of 0.45 and 0.12 respectively (p<0.01). **J-K.** SEM images of cells and collagen fiber distribution in a supercritical (**J**) and subcritical (**K**) samples. (For interpretation of the references to colour in this figure legend, the reader is referred to the web version of this article.)

bridges or tethers is a densified phase transition of ECM caused by buckling instability of fibers under cell induced compression [19]. This finding along with our images of collagen architecture for sub and supercritical cell densities suggest a link between material phase transition and appearance of cell network in compacting collagen discs.

3.3. Stochastic to deterministic transition in cell dynamics

The observations in the previous section prompted us to further investigate the mechanism of how the network formation is initiated and if there is a transition in cell dynamics as the process evolves. High resolution time-lapse imaging of a collagen disc seeded with cells above the critical density revealed that cells migrate in a random manner during the initial hours after seeding. As cell-cell interaction commenced, a striking network-like pattern emerged over time, which resulted in the compaction of the discs. Initially, individual cells displayed Brownian motion and probed surrounding microenvironment by extending small filopodia in random directions and by pulling on the adjacent fibers. This random protruding of filopodia ceased when a cell started interacting with a neighboring cell by extending longer protrusions and moving towards each other until the tips of the filopodia met. This gave rise to a network of cells which collectively contracted the gels (Fig. 4A-C, Supplementary Movie S.3). To quantify this stochastic to

deterministic transition in cell dynamics, we did a temporal mean-square displacement (tMSD, $MSD(\tau) \sim \tau^{\alpha}$) analysis of cell motion as described by Wylie et al. [41]. Here, we tracked the nucleus of the cell to quantify cell dynamics. Similar to the diffusion coefficient obtained from mean square displacement analysis of a particle, we extracted the parameter α as a continuous function of time, which allowed us to identify the transition from Brownian to processive dynamics. For purely Brownian motion, $\alpha = 1$, while $\alpha=2$ signifies ballistic motion. The details of the technique are described in the supplementary section (Supplementary Information S.3., Fig. S.3). For the cell tracked for tMSD analysis, initially α oscillated between 0.5-1 (approximately up to ~100 minutes) after forming the discs, signifying random dynamics. After that, when the cell started to approach a neighboring cell in a persistent manner, the value of α reached to approximately 1.6 after ~200 minutes. At ~240 minutes, we observed a drop in α which then started to increase again after ~265 minutes (Fig. 4E). When the cell moved towards the neighboring cell in a deterministic manner, the nucleus which is being tracked for the analysis moved along with the cell. As the cell reached close to the neighbor, the cell body became stationary at ~240 minutes while its filopodial protrusion started to extend towards that of the neighboring cell (Supplementary Movie S.5) up until ~265 minutes. During this time, the nucleus exhibited slight jiggling motion which is reflected in decreasing value of α to a super-diffusive regime. This is evident from the trajectory of
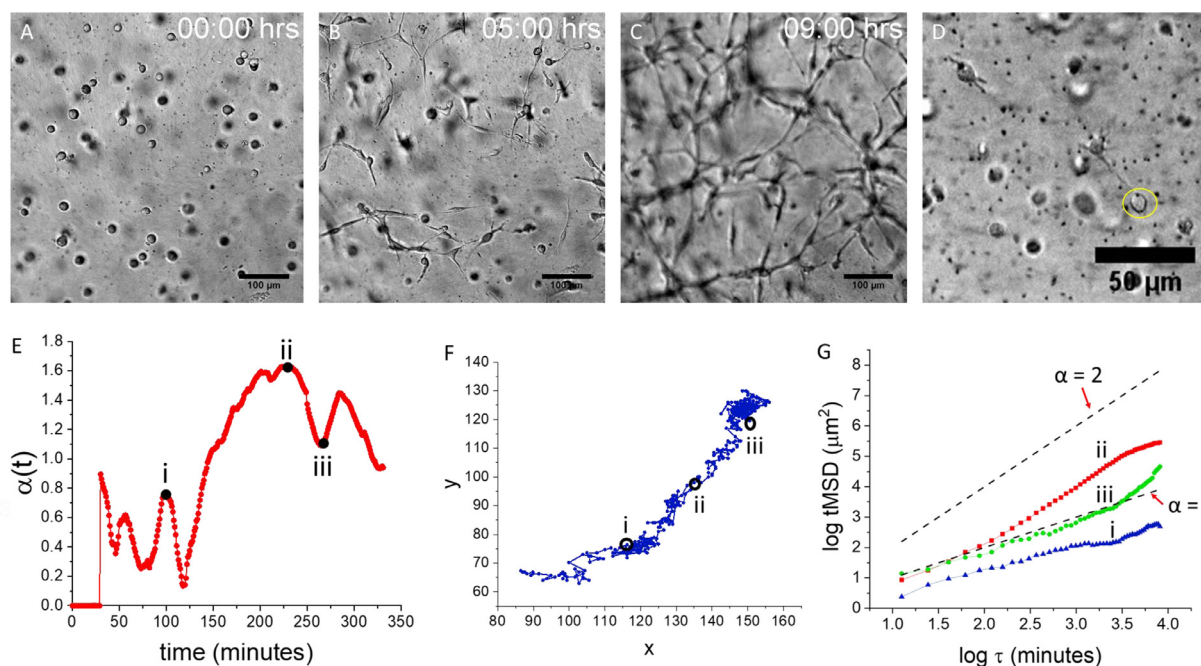
Fig. 4. Emergence of a network of cells as cell dynamics transitions from stochastic to deterministic at supercritical cell density. **A-C.** Bright field images of a FF discs at different time points showing the evolution of cell network from an initial uniform distribution of cells. Cell density is 1 million/ml. **D.** Zoomed-in bright field image of a representative cell (marked with yellow circle) whose position has been tracked over time for tMSD analysis, initial cell density is 1 million/ml. **E.** α vs time plot of the cell in D (yellow circle). The value of α oscillates between 0.5-1 until ~120 minutes when the cell exhibits Brownian motion, then α increases to ~1.6 over time as the cell switches to ballistic motion, which then start to decrease at ~240 minutes when the cell motion ceases temporarily. The parameter α is derived from the mean square displacement of a particle which indicates diffusive properties of the motion of the particle (i.e. Brownian or ballistic). $\alpha=1$ and $\alpha=2$ defines pure Brownian and pure ballistic motion respectively. **F.** Trajectory of the nucleus of the cell in D (yellow circle) in x-y plane. **G.** log-log plot of tMSD as a function of local time τ in each rolling time window τ_{max}. tMSD values at three time points t=100, 235, 265 minutes (marked by i, ii, iii respectively in E, F) are represented by the blue, red and green curves respectively, along with the lines of $\alpha=1$ and $\alpha=2$ (represented with black dashed lines). (For interpretation of the references to colour in this figure legend, the reader is referred to the web version of this article.)

the nucleus on the x-y plane, which shows random motion of the nucleus, followed by a ballistic trend, then again Brownian motion of the nucleus (Fig. 4F). After this period, the cell again started to move towards the neighbor, which explains the increase in α. The log-log plot of tMSD vs local time τ in each rolling window τ_{max} (details in Supplementary Information S.3) at three representative time points (t = 100, 235 and 265 minutes), along with lines representing $\alpha = 1$ and $\alpha = 2$ are shown in Fig. 4G. The distribution of α for large number (n = 20-80) of cells obtained from mean square displacement (MSD) analysis revealed the mean value of α was ~0.5 during the first 2 hours and it went up to ~1.6 as the disc started to compact (Supplementary Information S.3., Fig. S.4). The sub-diffusive behavior ($\alpha<1$) implies hindered Brownian motion of the cells during the first few hours after cell seeding. Our data suggest the existence of stochastic to deterministic transition in cell dynamics associated with the emergence of a global network of cells. The structural differences in collagen microarchitecture before and after compaction (Fig. 3) further hint that this network formation through cell-ECM interaction is a key mediator in regulating macroscopic compaction of the cell-ECM system. To test whether such network appears for other cell types while compacting collagen, we made tissues seeded with human colon cancer associated fibroblasts (CAF) and observed similar network formed by the cells (Supplementary Information S.10., Fig. S.11).

3.4. Local remodeling of ECM by sparsely populated cells is transient and reversible

Formation of collagen bands and fiber accumulation between mechanically interacting cells in 3D fibrous matrix mediated by contractile force has been reported in previous studies [25,32,42–

44]. The absence of such fiber accumulation in FF discs with subcritical cell density as found from our SHG images is rather remarkable (Fig. 3F). This prompted us to investigate the dynamics of individual cells with their surrounding matrix. As there is only negligible compaction in tissues with subcritical density over long time (Fig. 2C), these samples serve as a suitable model to study interaction between single cell and ECM when there is no cell-cell interaction. Time-lapse imaging revealed cells migrate randomly in the entire collagen disc without forming any network. Even when two cells come in close proximity at any point of time while moving randomly, they often move away from each other without interacting or contributing in compaction of the discs (Supplementary Movie S.4)-suggesting negligible effect of local remodeling of ECM by individual cells in global shrinking of the discs when cell density is below the critical regime.

To further understand how the matrix surrounding a single cell is deformed, we mixed 2 µm- diameter beads with collagen as tracers and tracked the motion of the beads in the vicinity of a cell over several hours. The strain between a pair of beads as a function of time was calculated from the initial distance L_0 and instantaneous distance L between the beads as $\varepsilon(t) = |L(t)-L_0|/L_0$ (Fig. 5A). We found that the cell induced a finite tensile strain on the beads, which then gradually reduced over time (Fig. 5B-D) as the cell retracted the filopodia and migrated to a new location (Supplementary Movie. S.6). This implies that there is no net deformation or permanent remodeling of the matrix. Cells only deform the local ECM reversibly in a transient fashion leaving no memory of its history. We repeated this bead pair test for five individual cells from different discs and found similar reversible strain dynamics (Supplementary Information S.4., Fig. S.5).
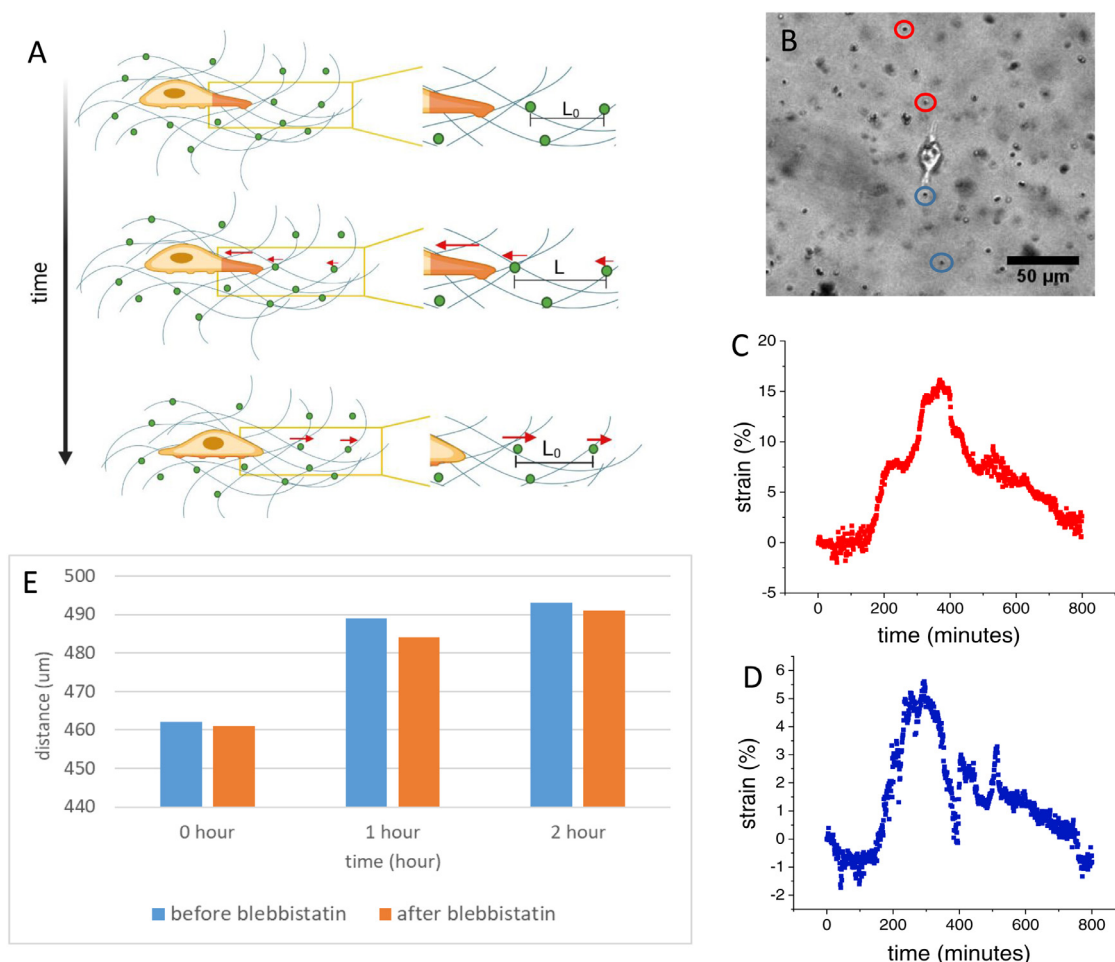
Fig. 5. Cells locally remodel ECM in a transient and reversible manner when cell density is below the critical value. **A.** Cartoon of the process of how local strain in ECM fibers is quantified as a function of time from tracking the distance between two tracer beads. **B.** Bright field image of a representative cell and beads in a collagen disc tracked for analysis of strain dynamics. **C-D.** Strain between two bead pairs as a function of time marked by the red circles (C) and blue circles (D) in B, respectively. Strain between the bead pair increases when the cell pulls them, and then reduces over time as the cell releases them. Initial cell seeding density in this experiment is 0.01 million/ml. **E.** Bar plot showing change of distance between two fixed points of a collagen disc as a function of time before and after adding Blebbistatin. Initial cell density was 1 million/ml.

The reversibility in ECM deformation is not just a local phenomenon observed between a single cell and ECM. In order to test the reversibility of ECM deformation on a global scale, we applied Blebbistatin in a partially compacted collagen disc and recorded rate of expansion of the disc by measuring the distance between two fixed points in the disc. The distance before and after adding the drug at different time points showed that the gel partially expands when drug is added (Fig. 5E, Supplementary Information S.7). This is supported by previous studies that reported similar partial expansion of collagen disc by applying Blebbistatin [32]. Application of Blebbistatin diminishes cell force by inhibiting myosin activity, indicating the aforementioned findings are governed by mechanical interactions. Next, we explored whether the cell-cell interaction is indeed mechanical.

3.5. Network formation is guided by mechanical cues

Cell-cell or cell-ECM interaction can be mediated through mechanical and/or biochemical signals. In most of the cases, these mediators work together, making it difficult to decouple one from the other. To assess the role of mechanical interaction of cell-ECM in network formation and phase transition in 3D tissue scaffolds, we populated our collagen discs with inert polystyrene (PS) beads (Fig. 6A). The beads have a diameter of 15 microns which is simi-

lar to the initial cell size (10-15 microns) and a much higher elastic modulus compared to the matrix. Unlike cells, the beads do not actively pull the surrounding ECM fibers. Rather they increase the local stiffness of the matrix, providing regions of higher stiffness that facilitate cell polarization and long range mechanical cell-cell interactions. We have validated this statement by taking an indirect approach to estimate the microscopic stiffness change in vicinity of a bead. We added 2 μm tracer beads to the cell-PS bead-collagen mixture and measured the strain as a function of time in the region between a cell and a PS bead using the displacement of the tracer beads by the applied contractile force of the cells-i.e., using the same technique described in Section 3.4. We found that the strain in the matrix in the vicinity of the PS bead reaches a maximum of approximately 30% when a nearby cell pulls towards a bead (Fig. 6C, Supplementary Movie S.7). This high strain indicates that local ECM response to cell force in the vicinity of a bead is governed by the nonlinear elastic properties of ECM, as supported by previous studies that reported the critical strain for nonlinear elastic response for collagen is approximately 10% [45]. A cell which mechanically probes the matrix by applying contractile force experiences a stiffness gradient towards the direction of a bead nearby. The beads are chemically inert, but guide cell motion and interaction in a purely mechanical way, decreasing the effective cell-cell distance. In other words, the bead presents itself
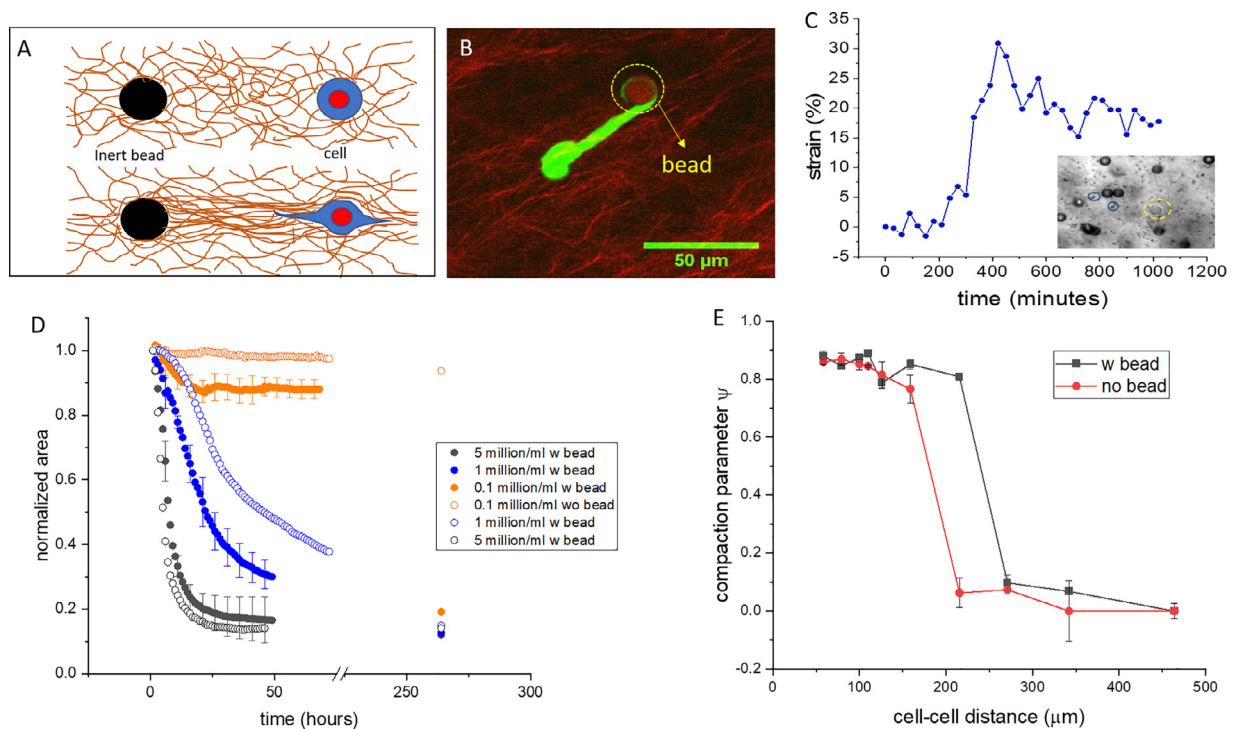
Fig. 6. Addition of inert 15 μm polystyrene (PS) beads shifts the phase transition point. **A.** Cartoon of cell-bead interaction in 3D collagen. Round cells polarize along the direction of bead. **B.** SHG and confocal imaging of live cells showing cell-bead interaction and cell orientation towards bead in 3D collagen. (Green-actin, Red- collagen). **C.** Strain in collagen fibers between a cell and nearby PS bead as a function of time, measured from tracer bead displacement, inset shows bright field image of the cell (yellow circle) and the tracer beads (blue circle) **D.** Area reduction rate of collagen discs of different cell densities with (filled circles) and without (empty circles) beads. Bead density is 1 million/ml (bead-bead gap 100 microns). For a given cell-cell distance, discs with beads compact faster and greater than control samples (no bead). **E.** critical cell-cell distance for compaction shifts to right when beads are added, collagen discs without bead show a sharp phase transition at a cell-cell distance of 150 microns, while discs with bead show phase transition at 210 microns. (For interpretation of the references to colour in this figure legend, the reader is referred to the web version of this article.)

as a mechanical cell to the neighboring living cell, effectively increasing the cell density and facilitating the network formation. To test whether the addition of beads perturbs the critical cell density for phase transition, we mixed 1 million/ml PS beads (bead-bead distance 100 microns) with cell-collagen mixture for various cell densities (0.01 to 5 million cells/ml) and observed the rate of reduction of disc area (Fig. 6D). We found that critical cell density decreases from 0.1 million cells/ml to 0.05 million cells/ml with the addition of beads. The corresponding critical cell-cell (living) distance for compaction increases from 160 μm to 210 microns (Fig. 6E). Actin-stained images reveal that cells indeed recognize the beads. They polarize towards the bead just as they do towards another live cell (Fig. 6B). This reveals that the addition of beads indeed shifts the critical length scale for compaction, implying that phase transition is guided by mechanical cues arising from cell-cell and cell-ECM interaction.

Cells respond to higher stiffness by exerting higher force on the surrounding ECM. Therefore, the addition of PS beads might increase the stiffness of the tissue and the observed shift in critical cell-cell distance might be the outcome of cell response to increase in overall elastic modulus of the matrix. To test if this is the case, we measured the stiffness of the cell-free collagen with and without adding PS beads using a PDMS based force sensor [33]. Stiffness measured by the sensor for control case and for collagen with PS beads were 6.4 nN/μm and 7.1 nN/μm respectively (Supplementary Information S.5), suggesting that the bead has a negligible contribution in overall stiffness of the tissue. Stiffness of the tissue increases as it compacts due to the strain-stiffening properties of collagen. To evaluate how stiffness increases as the cell-ECM network evolves, we have also measured the stiffness at different time points using the same sensor. We found that the stiffness in-

creases from 10 nN/μm on day 1 of culture to 50 nN/μm after three days (Supplementary Information, Fig. S.6).

4. Discussion

Our study reveals the existence of a phase transition and a critical cell-cell distance for compaction of 3D collagen gels mediated by contractile cells. From macroscopic compaction of tissue to gradually zooming into the mechanical interaction between neighboring cells and between single cell-ECM, our study shed light on the mechanism that links this critical length scale with transition from Brownian to ballistic motion in cells, as well as isotropic to anisotropic transition in collagen microstructure. Decoupling the mechanical cues from the cell-secreted biochemical factors by replacing cells with cell-sized inert PS beads, we have showed that the critical cell density for compaction shifts to a lower value. This suggests that compaction of tissue is facilitated by mechanical cues arising from the dynamic mechanical crosstalk between cell and 3D fibrous matrix. Similar shifts in phase transition due to external stimuli are also observed in other physical systems. For instance, ferromagnetic materials exhibit magnetism above Curie temperature under an external magnetic field [46], and the,-triple point of water shifts when pressure is applied [47]. Nonlinear elasticity of 3D fibrous matrix such as collagen and fibrin has been implicated in mediating cell-ECM interaction [24,43,48–50]. We found that the strain in the ECM along the direction of a PS bead resulting from an applied cell force reaches approximately 30% (Fig. 6C, Supplementary Movie S.7), which is much higher than the critical strain for nonlinear elasticity of collagen as reported by Sharma et al. [45]. This implies that the cell-cell mechanical interaction that leads to the formation of network of cells and their subsequent

compaction falls in the nonlinear elastic regime of collagen, and therefore nonlinear elasticity plays a key role in driving the process. We also found that the addition of PS beads has no significant effect in overall stiffness of the tissue (Supplementary Information S.5). This supports our assumption that the beads act as inclusions that increase stiffness locally, while mechanical properties of bulk collagen remain unperturbed, thus mediating local cell-cell mechanical interaction and shifting the critical distance for phase transition.

Our findings reveal that beyond the critical cell-cell distance, individual cells deform the matrix transiently and reversibly by pulling and releasing the adjacent fibers (Fig. 5). This suggests that in addition to nonlinear elasticity, time-dependent viscoelastic properties of collagen should be considered for further understanding of the mechanisms involved. The role of viscoelastic properties of ECM in regulating its interaction with cells in a tissue has recently come into focus [51]. A recent study has revealed that viscoelastic stress relaxation of collagen gives rise to local matrix reorganization that facilitates cell migration [52].

We have observed a stochastic to deterministic transition in cell motion prior to formation of cell network above the critical cell density. It is unclear how cells give up their random dynamics to switch to ballistic motion and the mechanistic origin of this persistent motion towards neighboring cells. It has been reported that substrate stiffness along with inherent diffusive properties of cells regulate cell-cell mechanical interaction in 2D linear elastic substrates [53,54]. As distance between two cells decreases, their 'interaction potential'- which is a measure of substrate compliance- increases, causing the cells to lose their Brownian dynamics and form stable contacts with each other [55]. The mechanical crosstalk is mediated by the deformation of the elastic substrate. In contrast, the nonlinear elastic properties of 3D fibrous matrix play a key role in establishing the dynamic mechanical crosstalk between cell and ECM. Single cells mechanically probe the surrounding microenvironment by extending actin-rich filopodial protrusions in random directions which originate from the stochastic actin dynamics [56]. This cell-ECM interaction is transient as observed from our results (Fig. 5). When the cells are nearby (above critical density), two protrusions from neighboring cells interact with each other by locally stretching the matrix. This interaction is also transient, as we observed from time-lapse imaging (Supplementary Movie S.3). Occasionally the facing protrusions synchronize their force when the local strain becomes high and collagen stiffness increases due to nonlinearity elasticity. This interaction leads to a transition from Brownian dynamics of cells to a stationary state when cell protrusions approach each other in a persistent feed forward way and results in a network across the entire matrix. This self-reinforcing mechanism that guides persistent cell migration arises from local gradients in collagen density [52] and tension anisotropy [57] mediated by cellular interaction.

Confocal images of cells that extend filopodia towards each other but whose filopodia tips have not meet and corresponding SHG images of stretched collagen fibers between them (Fig. 3A-C) imply that the fibers between two cells approaching each other are under tension until the tips of their filopodia meet. After the formation of the network, the cells contract with tensile forces along the protrusions employing the acto-myosin machinery, causing the fibers previously in tension to go under compression and buckle. This is supported by the confocal images of two live cells and fibers between them (Supplementary Information S.11) at two consecutive time points before compaction had begun. The fibers in between the cells were buckled but after the contact between the protrusions was severed, the fibers went back to their unbuckled state. This implies that the global contraction of the gel is mediated by compression and buckling of fibers, and the persistent cell motion towards each other and formation of filopodial connection precede fiber buckling and overall contraction of the gels.

The critical length scale for phase transition and compaction is governed by factors such as- cell-type and ECM properties as well. For example, formation of a cell-ECM network is also observed in Fibrin gels seeded with fibroblast cells [58]. In contrast, the process of forming blood clots by platelets by contracting fibrin gels is distinct from the compaction mechanism exhibited by fibroblasts. Unlike motile cells, platelets densify the fibrin network by pulling on the fibers transversely to their longitudinal axes, resulting in formation of fiber kinks [59]. Platelets also form aggregates as they come closer while contracting the fibrin gel in this manner. Future studies might address whether there exists a critical cell density and phase transition associated with contraction of fibrin gels. Gaining insight on the existence of a universal law of phase transition in multicellular systems could be beneficial for better understanding of emergent properties of such systems. These extrinsic factors (e.g. cell type) along with factors intrinsic to ECM (e.g. concentration, viscoelastic properties) together determine the critical length scale for collective action.

Taken together, our study sheds light on the underlying mechanism of emergence of collective behavior and an associated phase transition from a mechanics perspective. In a 3D microenvironment individual cells randomly probe the matrix by pulling and releasing the fibers. If a cell approaches a neighbor exercising similar dynamics, then the two neighbors may occasionally synchronize their pull on the ECM fibers between themselves. This perturbs the symmetry and homogeneity of the ECM for both the cells, biasing their interaction with the ECM along the direction towards each other resulting in ECM alignment and stiffening. The closer the cells are, the higher the likelihood of cell-cell interaction. Cells respond to the local stiffness gradients and polarize more towards each other while applying contractile forces on the ECM. Tensional stiffness between the cells continue to increase and the process evolves in a positive feed forward way [60]. The changes in ECM are now irreversible due to large local strains and possibly deposition of cross linkers by the cells. Once the interaction begins, the cells lose their "individuality" and their "free" random dynamics. They become locked in their relative positions. Each cell becomes part of a collective society working towards a common functionality, which is the compaction of the gel.

5. Conclusion

Emergence of collective behavior in biological systems has been a topic of intense research in developmental biology over the past decade. Understanding the precise mechanism of how a group of cells communicate and interact with each other to initiate collective behavior can be invaluable in assessing pathological conditions, as well as engineering functional tissue mimics. Our study in 3D *in vitro* tissue scaffold sheds light on the functional relationship between critical cell density for macroscopic compaction and structural phase transition in collagen. It also revealed that the phase transition originates from a complex dynamic interaction between cells and their ECM. A static view of interaction is not sufficient to explain the emergence of collective behavior in multi cellular systems.

Declaration of Competing Interest

The authors declare that they have no known competing financial interests or personal relationships that could have appeared to influence the work reported in this paper.

Acknowledgements

Supplementary materials

Supplementary material associated with this article can be found, in the online version, at doi:10.1016/j.actbio.2022.10.012.

References

[1] C.W. Reynolds, Flocks, herds and schools: a distributed behavioral model, in: Proceedings of the 14th Annual Conference on Computer Graphics and Interactive Techniques, Association for Computing Machinery, New York, NY, USA, 1987, pp. 25–34, doi:10.1145/37401.37406.

[2] D.J.T. Sumpter, J. Krause, R. James, I.D. Couzin, A.J.W. Ward, Consensus decision making by fish, Curr. Biol. 18 (2008) 1773–1777, doi:10.1016/j.cub.2008.09.064.

[3] C. Dambly-Chaudière, N. Cubedo, A. Ghysen, Control of cell migration in the development of the posterior lateral line: antagonistic interactions between the chemokine receptors CXCR4 and CXCR7/RDC1, BMC Dev. Biol. 7 (2007), doi:10.1186/1471-213X-7-23.

[4] A.S. Ghabrial, M.A. Krasnow, Social interactions among epithelial cells during tracheal branching morphogenesis, Nature 441 (2006) 746–749, doi:10.1038/nature04829.

[5] C.P. Heisenberg, Y. Bellaïche, XForces in tissue morphogenesis and patterning, Cell 153 (2013) 948, doi:10.1016/j.cell.2013.05.008.

[6] O. Aydin, A.P. Passaro, R. Raman, S.E. Spellicy, R.P. Weinberg, R.D. Kamm, M. Sample, G.A. Truskey, J. Zartman, R.D. Dar, S. Palacios, J. Wang, J. Tordoff, N. Montserrat, R. Bashir, M.T.A. Saif, R. Weiss, Principles for the design of multicellular engineered living systems, APL Bioeng. 6 (2022) 010903, doi:10.1063/5.0076635.

[7] B. Li, J.H.C. Wang, Fibroblasts and myofibroblasts in wound healing: force generation and measurement, J. Tissue Viability 20 (2011) 108–120, doi:10.1016/j.jtv.2009.11.004.

[8] F. Grinnell, Fibroblasts, myofibroblasts, and wound contraction, J. Cell Biol. 124 (1994) 401–404, doi:10.1083/jcb.124.4.401.

[9] Y. Hegerfeldt, M. Tusch, E.-B. Bröcker, P. Friedl, Collective cell movement in primary melanoma explants: plasticity of cell-cell interaction, β1-integrin function, and migration strategies1,2, Cancer Res. 62 (2002) 2125–2130.

[10] K. Campbell, F. Rossi, J. Adams, I. Pitsidianaki, F.M. Barriga, L. Garcia-Gerique, E. Batlle, J. Casanova, A. Casali, Collective cell migration and metastases induced by an epithelial-to-mesenchymal transition in Drosophila intestinal tumors, Nat. Commun. 10 (2019), doi:10.1038/s41467-019-10269-y.

[11] P. Friedl, D. Gilmour, Collective cell migration in morphogenesis, regeneration and cancer, Nat. Rev. Mol. Cell Biol. 10 (2009) 445–457, doi:10.1038/nrm2720.

[12] B. Emon, J. Bauer, Y. Jain, B. Jung, T. Saif, Biophysics of tumor microenvironment and cancer metastasis - a mini review, Comput. Struct. Biotechnol. J. 16 (2018) 279–287, doi:10.1016/j.csbj.2018.07.003.

[13] B. Szabó, G.J. Szöllösi, B. Gönci, Z. Jurányi, D. Selmeczi, T. Vicsek, Phase transition in the collective migration of tissue cells: Experiment and model, Phys. Rev. E Stat. Nonlin. Soft Matter Phys. 74 (2006), doi:10.1103/PhysRevE.74.061908.

[14] T. Vicsek, A. Czirók, E. Ben-Jacob, I. Cohen, O. Shochet, Novel type of phase transition in a system of self-driven particles, Phys. Rev. Lett. 75 (1995) 1226–1229, doi:10.1103/PhysRevLett.75.1226.

[15] D. Ito, H. Tamate, M. Nagayama, T. Uchida, S.N. Kudoh, K. Gohara, Minimum neuron density for synchronized bursts in a rat cortical culture on multi-electrode arrays, Neuroscience 171 (2010) 50–61, doi:10.1016/j.neuroscience.2010.08.038.

[16] G. Serini, D. Ambrosi, E. Giraudo, A. Gamba, L. Preziosi, F. Bussolino, Modeling the early stages of vascular network assembly, EMBO J. 22 (2003) 1771–1779, doi:10.1093/emboj/cdg176.

[17] T. Gregor, K. Fujimoto, N. Masaki, S. Sawai, The onset of collective behavior in social amoebae, Science 328 (2010) (1979) 1021–1025, doi:10.1126/science.1183415.

[18] H. Yang, A.F. Pegoraro, Y. Han, W. Tang, R. Abeyaratne, D. Bi, M. Guo, Configurational fingerprints of multicellular living systems, Proc. Natl. Acad. Sci. 118 (2021) e2109168118, doi:10.1073/pnas.2109168118.

[19] G. Grekas, M. Proestaki, P. Rosakis, J. Notbohm, C. Makridakis, G. Ravichandran, Cells exploit a phase transition to mechanically remodel the fibrous extracellular matrix, J. R. Soc. Interface 18 (2021), doi:10.1098/RSIF.2020.0823.

[20] L. Delaey, R. v Krishnan, H. Tas, H. Warlimont, Thermoelasticity, pseudoelasticity and the memory effects associated with martensitic transformations, J. Mater. Sci. 9 (1974) 1521–1535, doi:10.1007/BF00552939.

[21] E. Bell, B. Ivarsson, C. Merrill, Production of a tissue-like structure by contraction of collagen lattices by human fibroblasts of different proliferative potential in vitro, Proc. Natl. Acad. Sci. 76 (1979) 1274–1278, doi:10.1073/pnas.76.3.1274.

[22] D. Stopak, A.K. Harris, Connective tissue morphogenesis by fibroblast traction: I. Tissue culture observations, Dev. Biol. 90 (1982) 383–398, doi:10.1016/0012-1606(82)90388-8.

[23] C. Guidry, F. Grinnell, Studies on the mechanism of hydrated collagen gel reorganization by human skin fibroblasts, J. Cell Sci. 79 (1985) 67–81, doi:10.1242/jcs.79.1.67.

[24] J.P. Winer, S. Oake, P.A. Janmey, Non-linear elasticity of extracellular matrices enables contractile cells to communicate local position and orientation, PLoS One 4 (2009), doi:10.1371/journal.pone.0006382.

[25] A.S. Abhilash, B.M. Baker, B. Trappmann, C.S. Chen, V.B. Shenoy, Remodeling of fibrous extracellular matrices by contractile cells: predictions from discrete fiber network simulations, Biophys. J. 107 (2014) 1829–1840, doi:10.1016/j.bpj.2014.08.029.

[26] Q. Wen, P.A. Janmey, Effects of non-linearity on cell-ECM interactions, Exp. Cell. Res. 319 (2013) 2481–2489, doi:10.1016/j.yexcr.2013.05.017.

[27] K. Liu, M. Wiendels, H. Yuan, C. Ruan, P.H.J. Kouwer, Cell-matrix reciprocity in 3D culture models with nonlinear elasticity, Bioact. Mater. 9 (2022) 316–331, doi:10.1016/j.bioactmat.2021.08.002.

[28] S. Loerakker, C. Obbink-Huizer, F.P.T. Baaijens, S. Loerakker, C Obbink-Huizer, F.P.T. Baaijens, A physically motivated constitutive model for cell-mediated compaction and collagen remodeling in soft tissues, Biomech. Model. Mechanobiol. 13 (2014) 985–1001, doi:10.1007/s10237-013-0549-1.

[29] M.D. Stevenson, A.L. Sieminski, C.M. McLeod, F.J. Byfield, V.H. Barocas, K.J. Gooch, Pericellular conditions regulate extent of cell-mediated compaction of collagen gels, Biophys. J. 99 (2010) 19–28, doi:10.1016/j.bpj.2010.03.041.

[30] V.H. Barocas, R.T. Tranquillo, An anisotropic biphasic theory of tissue-equivalent mechanics: the interplay among cell traction, fibrillar network deformation, fibril alignment, and cell contact guidance, J. Biomech. Eng. 119 (1997) 137–145, doi:10.1115/1.2796072.

[31] Z. Feng, Y. Wagatsuma, M. Kikuchi, T. Kosawada, T. Nakamura, D. Sato, N. Shirasawa, T. Kitajima, M. Umezu, The mechanisms of fibroblast-mediated compaction of collagen gels and the mechanical niche around individual fibroblasts, Biomaterials 35 (2014) 8078–8091, doi:10.1016/j.biomaterials.2014.05.072.

[32] P. Fernandez, A.R. Bausch, The compaction of gels by cells: a case of collective mechanical activity, Integr. Biol. 1 (2009) 252–259, doi:10.1039/b822897c.

[33] B. Emon, Z. Li, S.H. Joy, U. Doha, F. Kosari, M. Taher, A. Saif, A novel method for sensor-based quantification of single/multicellular force dynamics and stiffening in 3D matrices, 2021. https://www.science.org.

[34] M. Elhebeary, M.A.B. Emon, O. Aydin, M.T.A. Saif, A novel technique for in situ uniaxial tests of self-assembled soft biomaterials, Lab Chip 19 (2019) 1153–1161, doi:10.1039/c8lc01273c.

[35] J.-Y. Tinevez, N. Perry, J. Schindelin, G.M. Hoopes, G.D. Reynolds, E. Laplantine, S.Y. Bednarek, S.L. Shorte, K.W. Eliceiri, TrackMate: An open and extensible platform for single-particle tracking, Methods 115 (2017) 80–90, doi:10.1016/j.ymeth.2016.09.016.

[36] R. Rezakhaniha, A. Agianniotis, J.T.C. Schrauwen, A. Griffa, D. Sage, C.V.C. Bouten, F.N. van de Vosse, M. Unser, N. Stergiopulos, Experimental investigation of collagen waviness and orientation in the arterial adventitia using confocal laser scanning microscopy, Biomech. Model. Mechanobiol. 11 (2012) 461–473, doi:10.1007/s10237-011-0325-z.

[37] C.B. Raub, V. Suresh, T. Krasieva, J. Lyubovitsky, J.D. Mih, A.J. Putnam, B.J. Tromberg, S.C. George, Noninvasive assessment of collagen gel microstructure and mechanics using multiphoton microscopy, Biophys. J. 92 (2007) 2212–2222, doi:10.1529/biophysj.106.097998.

[38] D. Vader, A. Kabla, D. Weitz, L. Mahadevan, Strain-induced alignment in collagen gels, PLoS One 4 (2009), doi:10.1371/journal.pone.0005902.

[39] Q. Shi, R.P. Ghosh, H. Engelke, C.H. Rycroft, L. Cassereau, J.A. Sethian, V.M. Weaver, J.T. Liphardt, Rapid disorganization of mechanically interacting systems of mammary acini, Proc. Natl. Acad. Sci. USA 111 (2014) 658–663, doi:10.1073/pnas.1311312110.

[40] E. Ban, J.M. Franklin, S. Nam, L.R. Smith, H. Wang, R.G. Wells, O. Chaudhuri, J.T. Liphardt, V.B. Shenoy, Mechanisms of plastic deformation in collagen networks induced by cellular forces, Biophys. J. 114 (2018) 450–461, doi:10.1016/j.bpj.2017.11.3739.

[41] W.W. Ahmed, B.J. Williams, A.M. Silver, T.A. Saif, Measuring nonequilibrium vesicle dynamics in neurons under tension, Lab Chip 13 (2013) 570–578, doi:10.1039/c2lc41109a.

[42] A. Malandrino, M. Mak, X. Trepat, R.D. Kamm, Non-elastic remodeling of the 3D extracellular matrix by cell-generated forces, BioRxiv. (2017) 193458. doi:https://doi.org/10.1101/193458.

[43] R.S. Sopher, H. Tokash, S. Natan, M. Sharabi, O. Shelah, O. Tchaicheeyan, A. Lesman, Nonlinear elasticity of the ECM fibers facilitates efficient intercellular communication, Biophys. J. 115 (2018) 1357–1370, doi:10.1016/j.bpj.2018.07.036.

[44] A. Malandrino, X. Trepat, R.D. Kamm, M. Mak, Dynamic filopodial forces induce accumulation, damage, and plastic remodeling of 3D extracellular matrices, PLoS Comput. Biol. 15 (2019) e1006684 -, doi:10.1371/journal.pcbi.1006684.

[45] A. Sharma, A.J. Licup, K.A. Jansen, R. Rens, M. Sheinman, G.H. Koenderink, F.C. Mackintosh, Strain-controlled criticality governs the nonlinear mechanics of fibre networks, Nat. Phys. 12 (2016) 584–587, doi:10.1038/nphys3628.

[46] T. Moriya, Nuclear magnetic relaxation near the curie temperature, Prog. Theor. Phys. 28 (1962) 371–400, doi:10.1143/PTP.28.371.

[47] A. Faghri, Y. Zhang, 1 - Introduction to transport phenomena, in: A. Faghri, Y. Zhang (Eds.), Transport Phenomena in Multiphase Systems, Academic Press, Boston, 2006, pp. 1–106, doi:10.1016/B978-0-12-370610-2.50006-4.

[48] P.L. Chandran, V.H. Barocas, Microstructural mechanics of collagen gels in confined compression: poroelasticity, viscoelasticity, and collapse, J. Biomech. Eng. 126 (2004) 152–166, doi:10.1115/1.1688774.

[49] P.A. Janmey, M.E. McCormick, S. Rammensee, J.L. Leight, P.C. Georges, F.C. MacKintosh, Negative normal stress in semiflexible biopolymer gels, Nat. Mater. 6 (1) (2007) 48–51 6 (2006), doi:10.1038/nmat1810.

[50] P. Fernández, P.A. Pullarkat, A. Ott, A master relation defines the nonlinear viscoelasticity of single fibroblasts, Biophys. J. 90 (2006) 3796–3805, doi:10.1529/biophysj.105.072215.

[51] O. Chaudhuri, J. Cooper-White, P.A. Janmey, D.J. Mooney, V.B. Shenoy, Effects of extracellular matrix viscoelasticity on cellular behaviour, Nature 584 (2020) 535–546, doi:10.1038/s41586-020-2612-2.

[52] A.G. Clark, A. Maitra, C. Jacques, M. Bergert, C. Pérez-González, A. Simon, L. Lederer, A. Diz-Muñoz, X. Trepat, R. Voituriez, D.M. Vignjevic, Self-generated gradients steer collective migration on viscoelastic collagen networks, Nat. Mater. (2022) 1–11 2022, doi:10.1038/s41563-022-01259-5.

[53] C.A. Reinhart-King, M. Dembo, D.A. Hammer, Cell-cell mechanical communication through compliant substrates, Biophys. J. 95 (2008) 6044–6051, doi:10.1529/biophysj.107.127662.

[54] S. Bose, P.S. Noerr, A. Gopinathan, A. Gopinath, K. Dasbiswas, Collective states of active particles with elastic dipolar interactions, n.d.

[55] S. Bose, K. Dasbiswas, A. Gopinath, Matrix stiffness modulates mechanical interactions and promotes contact between motile cells, (2021). doi:10.3390/biomedicines9040428.

[56] Y. Lan, G.A. Papoian, The stochastic dynamics of filopodial growth, Biophys. J. 94 (2008) 3839, doi:10.1529/BIOPHYSJ.107.123778.

[57] F. Alisafaei, D. Shakiba, L.E. Iannucci, M.D. Davidson, K.M. Pryse, P.-H.G. Chao, J.A. Burdick, S.P. Lake, E.L. Elson, V.B. Shenoy, G.M. Genin, # Affiliations, Tension anisotropy drives phenotypic transitions of cells via two-way cell-ECM feedback, BioRxiv. (2022) 2022.03.13.484154. doi:10.1101/2022.03.13.484154.

[58] S. Natan, Y. Koren, O. Shelah, S. Goren, A. Lesman, Long-range mechanical coupling of cells in 3D fibrin gels, Mol. Biol. Cell 31 (2020) 1474–1485, doi:10.1091/mbc.E20-01-0079.

[59] O.V. Kim, R.I. Litvinov, M.S. Alber, J.W. Weisel, Quantitative structural mechanobiology of platelet-driven blood clot contraction, Nat. Commun. 8 (2017) 1274, doi:10.1038/s41467-017-00885-x.

[60] M.S. Hall, F. Alisafaei, E. Ban, X. Feng, C.Y. Hui, V.B. Shenoy, M. Wu, Fibrous nonlinear elasticity enables positive Mechanical feedback between cells and ECMs, Proc. Natl. Acad. Sci. USA 113 (2016) 14043–14048, doi:10.1073/pnas.1613058113.